Journal of Geosciences, 65 (2020), 121–138 DOI: 10.3190/jgeosci.305

Original paper

Was the Tynong Batholith, Lachlan Orogen, Australia, extremely hot? Application of pseudosection modelling and TitaniQ geothermometry

Kamal Raj REGMI[1*], Pavlína HASALOVÁ[2], Ian A. NICHOLLS[3]

[1] *School of Geography, Earth Sciences and Environment, the University of the South Pacific, Laucala Campus, Private Bag, Suva, Fiji; kamalregminp@yahoo.com*
[2] *Centre for Lithospheric Research, Czech Geological Survey, Klárov 3, 118 21 Prague 1, Czech Republic*
[3] *School of Earth, Atmosphere and Environment, Clayton Campus, Monash University, Melbourne, VIC 3800, Australia*
[*] *Corresponding author*

Tonalites to granites of the Tynong Batholith, Lachlan Orogen, southeastern Australia as well as enclaves within them contain primary clino- and orthopyroxenes. These plutons produced very broad (2–10 km) contact aureoles that contain an anatectic zone within metagreywackes. The very broad contact aureoles can be related to the 3-D shapes of the plutons and we assume that the Cpx and Opx are remnants of higher temperature crystallization that were preserved due to water loss or low water content in the magma. Estimates of P and T based on x(Fe) values for coexisting cordierite and biotite in P–T pseudosections for a typical migmatitic hornfels, providing minimum temperature of pluton emplacement, indicate emplacement of the Toorongo tonalite at 4–10 km (1–3 kbar) and 680–750 °C. However, the isopleths of An content of plagioclase indicate depths of up to 14 km at 660–740 °C. We suggest that plagioclase was partially re-equilibrated during melt loss and post-emplacement decompression.

Cathodoluminescence (CL) imaging shows that quartz both in the tonalites and hornfels is typically zoned from higher Ti contents in cores to lower in the margins, suggesting a response to falling temperature. Calculated temperatures for quartz crystallization using a Ti-in-quartz thermometer calibrated for 2.5 kbar gave a wide range of values between 900 and 500 °C. This suggests that although the granitoids contain two pyroxenes and have produced a broad contact aureole, they were not emplaced at temperatures as high as previously inferred.

Keywords: TitaniQ, pseudosection modelling, Tynong Batholith, P–T estimation
Received: 26 October 2018; accepted: 25 June 2020; handling editor: J. M. Hora
The online version of this article (doi: 10.3190/jgeosci.305) contains supplementary electronic material.

1. Introduction and aims

The Tynong Batholith is located in the Melbourne Zone of the eastern Lachlan Orogen. The Toorongo Pluton is one of the largest. Based upon its partially melted contact aureole, and on the presence of Cpx and pseudomorphs after Opx in the granitoids as well as in its enclaves, it was probably the hottest pluton among the Tynong Province granitoids (Regmi 2012; Regmi et al. 2016). The Toorongo, Tanjil Bren and Baw Baw plutons have produced an unusually broad (2–10 km wide) high-temperature contact aureole, including a spectacular zone of partial melting and deformation developed within the quartz-rich metasedimentary country rocks, recording their thermal evolution during and after intrusion of apparently very hot granitic magmas. Although much work has been done on the geochemistry, petrography and evolution of the Tynong Batholith (e.g. Regmi 2012; Clemens and Bezuidenhout 2014; Clemens et al. 2016; Regmi et al. 2016), no previous P–T estimates are available for it. This paper describes the pressure–temperature results of pseudosection modelling of the mineral assemblage of an anatectic Toorongo contact aureole hornfels to infer the minimum temperature of pluton emplacement. It then outlines the results of the study of the cathodoluminescence of quartz for a hybrid quartz diorite with quartz ocelli from the Tynong Pluton, a granodiorite from the Toorongo Pluton and the hornfels used for pseudosection modelling. This leads to temperature determination using Ti-in-quartz geothermometry to test the applicability of the method and to infer the temperature of emplacement of the Tynong Batholith.

2. Geological setting

The Tynong Province granites lie within the Melbourne Tectonic Zone (Vandenberg et al. 2000; Rossiter 2003) of the Lachlan Orogen, northeast of Melbourne, Australia. The Tynong Batholith belongs to the Central Granite Superprovince of Victoria. It is the largest of a group of Late Devonian (~370 Ma) granitic complexes (Gray

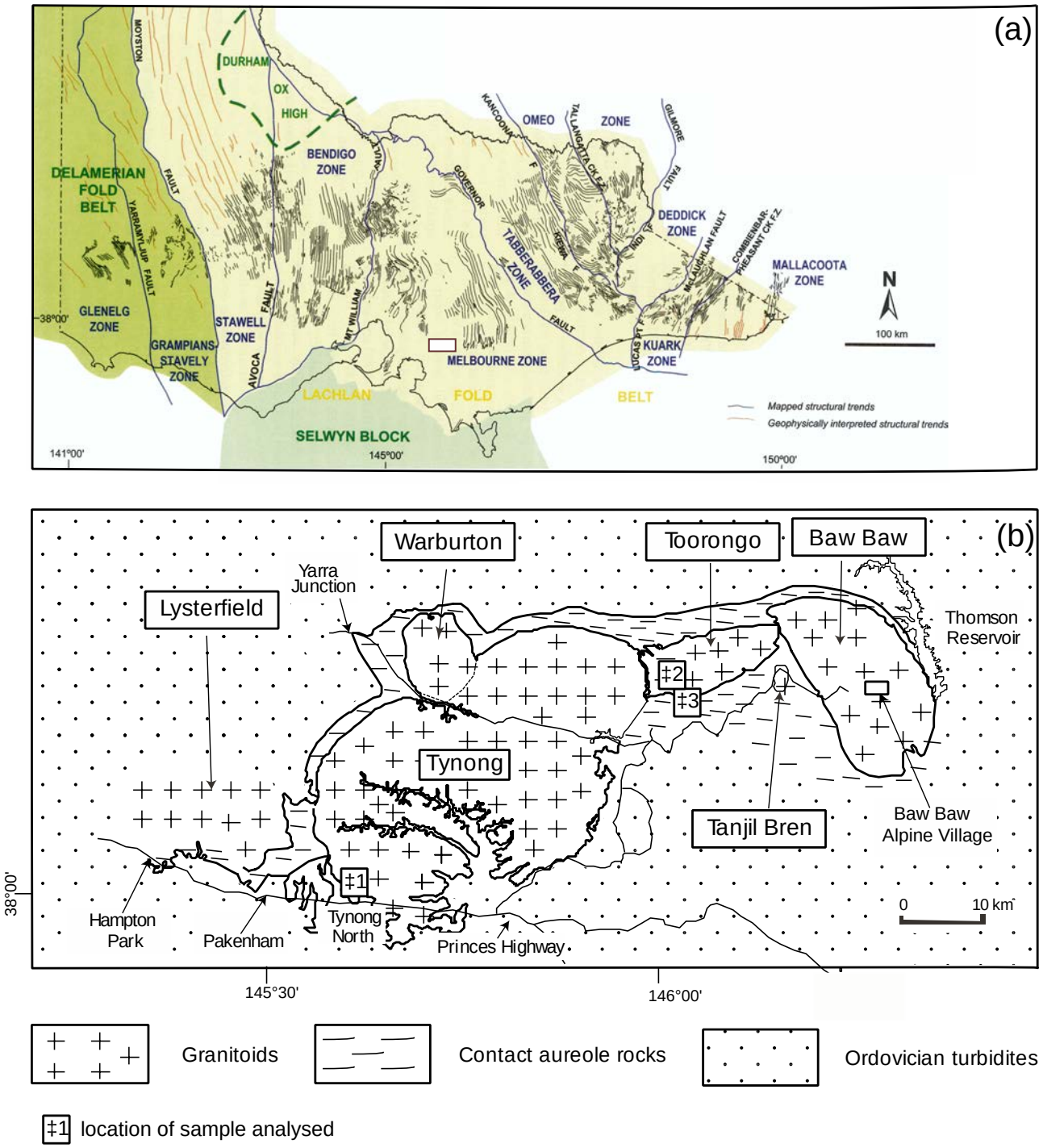

Fig. 1a – Geological map of the Lachlan Fold Belt, Victoria, Australia (modified after Vandenberg et al. 2000). **b** – Geological map of the Tynong Province granitoids and location of the samples analyzed: ‡1 – sample 802-1, ‡2 – sample 203, and ‡3 – sample 201.

and Kemp 2009), including at least five plutons (i.e., Lysterfield, Tynong, Toorongo, Tanjil Bren and Baw Baw plutons; Fig. 1), which are exposed in the high country between the Melbourne metropolitan area in the west and the Thomson Reservoir in the east. Most of the granitoids are metaluminous, the Tanjil Bren Pluton and more felsic samples of the Tynong Pluton being slightly peraluminous (Regmi 2012). The geology of the Tynong Batholith has been outlined by Regmi (2012), Clemens and Bezuidenhout (2014), Clemens et al. (2016) and Regmi et al. (2016). The Batholith was intruded into strongly folded Early Ordovician to Early Devonian turbidite sequences. Radiometric dating of the Toorongo Pluton has yielded a K–Ar biotite cooling age of 371 ± 6

Ma (Bowen 1975; McKenzie et al. 1984) and a U–Pb zircon age of 375 ± 2 Ma (Regmi 2012; Regmi et al. 2016).

3. Application of pseudosection modelling and TitaniQ geothermometry in P–T estimation

Pseudosections (Powell and Holland 1993; Connolly and Petrini 2002) allow detailed determination of pressure–temperature (P–T) for peak metamorphic conditions or metamorphic paths, and this approach has proven especially useful in unravelling the evolution of a variety of rock complexes. P–T pseudosections have proved to be a popular and powerful means of predicting and explaining mineral parageneses of metamorphic and igneous rocks (Vance and Holland 1993; Marmo et al. 2002). Estimation of the P–T conditions of melting of contact aureole rocks can give information about the minimum emplacement temperature of a pluton that caused melting.

Quartz is typically one of the last phases to crystallize from granitic melt, and given sufficient time, diffusion of Ti in quartz (Cherniak et al. 2007) may partially re-equilibrate small grains or fine-scale zoning at these temperatures. Therefore, TitaniQ-derived temperatures from crystal rims can reasonably be regarded as minimum emplacement temperatures, with the potential for preservation of earlier magmatic history in crystal interiors if cooling was rapid enough to prevent diffusive re-equilibration.

Over a wide range of pressures and temperatures Ti^{4+} substitutes in the Si^{4+} site of quartz (Wark and Watson 2006; Thomas et al. 2010). The colour of quartz and its luminescence reflect the incorporation of trace elements and the lattice defects they create (Cherniak et al. 2007). The growth history of quartz is preserved in zoning of individual grains, often observable by variation in CL intensity (Holness and Watt 2001), and in Ti zonation; and it can provide information about magmatic processes and the crystallisation history of granites (Cherniak et al. 2007).

The CL emission intensity correlates with Ti concentration in quartz and this in turn relates to the temperature of crystallisation of igneous quartz (Wark and Watson 2006; Wiebe et al. 2007). High pressure also favors Ti incorporation into quartz (Müller et al. 2002; Thomas et al. 2010; Huang and Audetat 2012).

For the temperature range from 600 to 1000 °C and at a pressure of 10 kbar, Wark and Watson (2006) established the following relationship:

$$\mathrm{T}(^{\circ}C) = -3765 / \left[\log\left(X_{Qtz}^{Ti} / a\mathrm{TiO}_2\right) - 5.69\right] - 273 \quad (1)$$

where X_{Qtz}^{Ti} is the titanium content of quartz in ppm and $a\mathrm{TiO}_2$ is TiO_2 activity relative to that required for rutile saturation. Thomas et al. (2010) explored the effect of pressure on the TitaniQ geothermometer and derived an expression for pressures of 5–20 kbar and temperatures of 700–940 °C as:

$$\mathrm{RT}\ln\left(X_{Qtz}^{TiO_2}\right) = -60952 + 1.520 \times T - 1741 \times P + RT \times \ln\left(a\mathrm{TiO}_2\right) \quad (2)$$

where R is the gas constant 8.3145 $J \times K^{-1} \times mol^{-1}$, and $X_{Qtz}^{TiO_2}$ is expressed as molar fraction of TiO_2.

Huang and Audetat (2012) formulated a new calibration of the Ti-in-quartz thermometer (TitaniQ) as:

$$\log\mathrm{Ti}\ (\mathrm{ppm}) = -0.27943 \times 10^4 / T - 660.53 \times \left(P^{0.35} / T\right) + 5.6459 \quad (3)$$

Equation (3) was calibrated for pressures of 0.1–10 kbars.

More recently, Zhang et al. (2020) re-calibrated TitaniQ and derived an expression as:

$$\log\left(C_{Ti}^{Qtz}\right) = 5.3226 - 1948.4 / T - 981.4 \times P^{0.2} / T \quad (4)$$

where C_{Ti}^{Qtz} is the Ti concentration in quartz in ppm, T is in Kelvin and P is in kbar as in expressions 2–3.

As expression 1 (Wark and Watson 2006) does not consider the effect of pressure on quartz crystallization temperature, we do not calculate temperatures using this calibration. Similarly, for the Thomas et al. (2010) equation, 2.5 kbar (the pressure at which most probably the studied granitoids were emplaced) is outside the calibration range, and therefore not used for calculation. Moreover, using the Bishop Tuff as a case, Wilson et al. (2012) criticized that the expression calibrated by Thomas et al. (2010; expression 2 above) yields an inaccurate value of third parameter (either P, or T or $a\mathrm{TiO}_2$) even if the values of the other two are taken correctly. So, we used expressions (3) and (4) to calculate temperatures of quartz crystallization.

4. Samples studied

4.1. Sample for pseudosection modelling (sample 201)

The sample (201) used for pseudosection modelling is from the hornfels within a turbiditic sequence that forms part of the Toorongo thermal metamorphic aureole (Fig. 1) collected 15–20 m from the granite contact (coordinates: 146°06'11"E, 37°50'05"S). It was also used for temperature estimation by TitaniQ.

Fig. 2 Outcrop of the Toorongo contact aureole hornfels/migmatite with layer-parallel and cross-cutting neosomes. The white material is neosome while the grey/black material is mesosome. This outcrop is ~10 m away from the contact with the intrusion.

The hornfelses of the Toorongo contact aureole have been partially melted (Fig. 2) to form a narrow (~100 m wide) zone of migmatitic rocks with neosomes oriented mostly parallel to the bedding. The more distal country rocks had been of very low metamorphic grade (prehnite–pumpellyite facies) before they were heated intensively in the granite aureole, melting partially to produce migmatitic rocks (Regmi et al. 2016).

The hornfels has a fine-grained mesosome composed of K-feldspar (50–60 vol. %), quartz (15–20 %) and biotite (15 %) with subordinate amounts of plagioclase and muscovite (Fig. 3). Quartz is the dominant mineral of the neosome (Fig. 4b), which is composed of quartz (50–60 vol. %), cordierite (15–20 %), K-feldspar (10–15 %), biotite, muscovite (10–15 %), and plagioclase (5–10 %). In contrast to the mesosome, the neosome is coarser grained and biotite flakes are less abundant. Some characteristic features of different minerals in the mesosome and neosome are illustrated below:

Plagioclase is found only in the neosome. It is mostly interstitial, subhedral to euhedral and shows polysynthetic twinning and sporadic zoning. Its composition varies between $An_{28}Ab_{71}$ and $An_{45}Ab_{55}$ for the rims and $An_{36}Ab_{64}$ to $An_{44}Ab_{56}$ for the cores (Tab. 1).

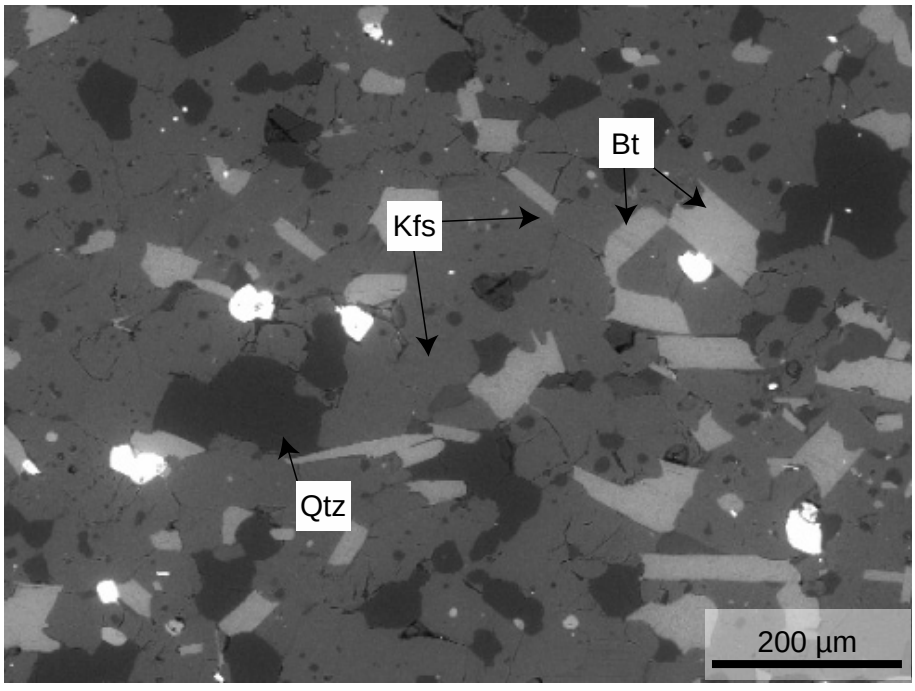

Fig. 3 Back-scattered electron image of the mesosome of the hornfels (sample 201) showing the dominance of Kfs.

Biotite in the mesosome has smaller grain size than in the neosome, in which it is present in smaller amounts and is mostly euhedral. There is no major difference between the x(Fe/(Fe + Mg)) of biotite in the mesosome (from 0.60 to 0.62) and in the neosome (0.61). The TiO_2 content of biotite varies from 3.3 to 3.8 wt. % in the mesosome and 2.7 to 3.5 wt. % in the neosome (Tab. 2).

Muscovite is present mostly in the neosome (Fig. 4b) although traces are also observed in the mesosome. Some of the muscovite flakes are skeletal and they show a resorbed tex-

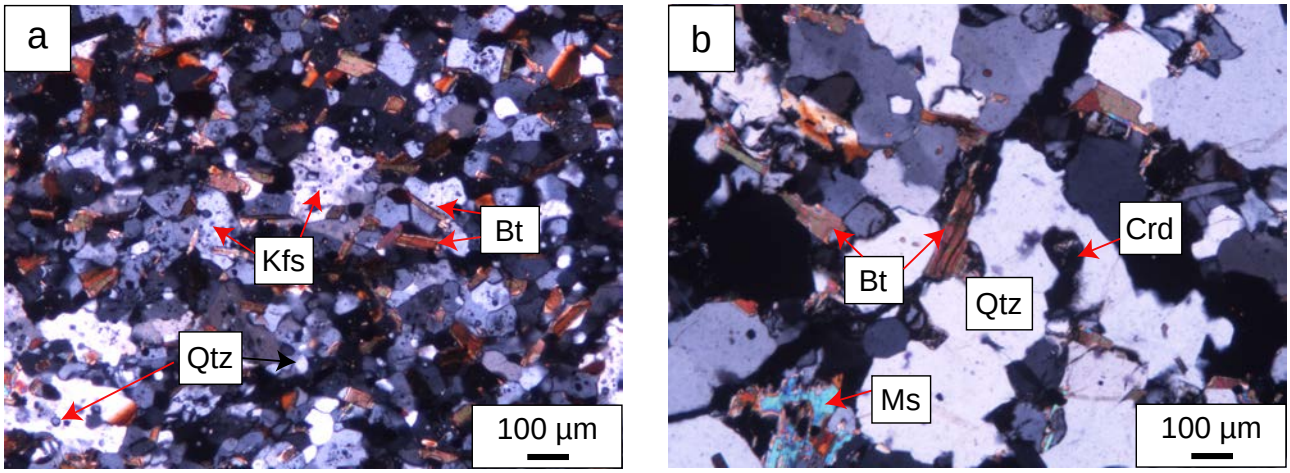

Fig. 4 Representative photomicrographs of the hornfels (crossed polars): **a** – Fine-grained mesosome; **b** – Coarse-grained neosome with cordierite.

ture that is characteristic of disequilibrium with the melt. The x(Fe/(Fe + Mg)) of muscovite from the neosome ranges from 0.50 to 0.54 (Tab. 3).

K-feldspar is mostly poikilitic and microperthitic, and it encloses rounded quartz crystals in the mesosome, whereas it is free of inclusions in the neosome. The composition of K-feldspar in the mesosome varies from $Or_{79}Ab_{21}$ to $Or_{84}Ab_{16}$ (Tab. 3). In the neosome K-feldspar is sometimes myrmekitic.

Cordierite is pinitized and it is present only in the neosome (Fig. 4b). It is mostly rounded but is locally prismatic. It contains no sillimanite (fibrolite) inclusions and is interpreted to be a peritectic mineral resulting from the melting reaction that produced the neosomes. In most migmatites, cordierite is associated with muscovite but when biotite is found together with it, biotite is anhedral. The x(Fe/(Fe + Mg)) of cordierite varies from 0.47 to 0.48, cores having slightly lower values than rims (Tab. 3).

Quartz in the mesosome is of two types. Small rounded quartz grains are included in K-feldspar (Fig. 4a), while others have triple junctions and are coarser grained than inclusions of quartz. Quartz in the neosome is larger than that in the mesosome.

Zircon and opaque minerals (chalcopyrite, pyrrhotite, pentlandite and ilmenite) are the accessories as identified in the thin and polished sections.

Tab. 1 Plagioclase analyses from neosome (wt. % and apfu)

No	11-c	12-r	23-c	24-r	32-c	42-r	52-r
SiO_2	59.21	60.65	56.85	56.29	57.32	58.50	58.29
TiO_2	0.02	0.00	0.00	0.03	0.01	0.01	0.00
Cr_2O_3	0.00	0.01	0.02	0.00	0.00	0.01	0.00
Al_2O_3	25.64	24.31	26.70	27.04	26.41	25.54	25.70
FeO	0.12	0.17	0.06	0.09	0.06	0.11	0.05
MnO	0.00	0.00	0.03	0.00	0.00	0.02	0.00
NiO	0.00	0.03	0.03	0.01	0.00	0.00	0.06
MgO	0.01	0.00	0.00	0.01	0.00	0.00	0.01
CaO	7.41	5.93	9.05	9.28	8.56	7.38	7.84
Na_2O	7.33	8.16	6.36	6.31	6.79	7.41	7.14
K_2O	0.13	0.15	0.14	0.12	0.11	0.10	0.16
Total	99.89	99.44	99.25	99.19	99.34	99.12	99.27
Cations (Fe^{2+}/Fe^{3+} charge balance)							
Si	2.65	2.71	2.57	2.54	2.58	2.63	2.62
Ti	0.00	0.00	0.00	0.00	0.00	0.00	0.00
Cr	0.00	0.00	0.00	0.00	0.00	0.00	0.00
Al	1.35	1.28	1.42	1.44	1.40	1.35	1.36
Fe^{3+}	0.00	0.01	0.00	0.00	0.00	0.00	0.00
Fe^{2+}	0.00	0.00	0.00	0.00	0.00	0.00	0.00
Mn	0.00	0.00	0.00	0.00	0.00	0.00	0.00
Ni	0.00	0.00	0.00	0.00	0.00	0.00	0.00
Mg	0.00	0.00	0.00	0.00	0.00	0.00	0.00
Ca	0.35	0.28	0.44	0.45	0.41	0.36	0.38
Na	0.64	0.71	0.56	0.55	0.59	0.65	0.62
K	0.01	0.01	0.01	0.01	0.01	0.01	0.01
Total	5.00	5.00	5.00	5.00	5.00	5.00	5.00
End members							
Anorthite	0.36	0.28	0.44	0.45	0.41	0.35	0.37
Albite	0.64	0.71	0.56	0.55	0.59	0.64	0.62
Orthoclase	0.01	0.01	0.01	0.01	0.01	0.01	0.01
Total end members	1.00	1.00	1.00	1.00	1.00	1.00	1.00

r – rim, c – core

Based on the mineralogy and textures, the melting reaction producing this migmatite is inferred to be (Otamendi and Patiño Douce 2001):

Qtz + Pl+ Bt ± Sil ± H_2O= melt ± Kfs+ Grt/Crd + Ilm

One significant issue with the use of pseudosections (not only) for this occurrence is the possible loss of melt during anatexis. This implies that the chemistry of the sample changed during metamorphism, adding a third unconstrained variable to the system. The field relationships (Fig. 2) and petrography of the hornfels suggest local and limited melting and consequently little melt loss. However, the richness in Al and Fe of the migmatites may suggest significant lowering of SiO_2 due to melt loss.

4.2. Samples for TitaniQ geothermometry

4.2.1. Tynong hybrid diorite (sample 802-1)

This sample was collected in a quarry wall of the Tynong North Quarry showing abundant magmatic structures and textures interpreted to indicate mingling between felsic and mafic magmas. It is composed of plagioclase, K-feldspar, quartz, hornblende, biotite, zircon, apatite, sphene and opaque minerals. This sample is slightly chloritized. Plagioclase and quartz are sometimes surrounded by hornblende, forming ocelli. This sample was chosen to study the distribution and zoning pattern of Ti in quartz grains associated with ocelli to estimate the temperature of ocelli development formed by magma mingling (Regmi 2012; Regmi et al. 2016) and to investigate any effect of Hbl on Ti distribution.

4.2.2. Toorongo granodiorite (sample 203)

The Toorongo granodiorite sampled near to the contact with hornfels is hypidiomorphic, coarse-grained and it is mainly composed of plagioclase, K-feldspar, quartz, hornblende and biotite as major minerals, and apatite, zircon, sphene and opaque phases as accessory minerals, with epidote as a secondary mineral.

Tab. 2 Biotite analyses (wt. % and apfu)

No	1-M	2-M	4-M	5-L	7-L	8-L	13-M	14-M	15-M
SiO_2	34.38	34.14	34.62	34.70	34.51	34.35	34.35	34.09	34.84
TiO_2	3.57	3.81	3.34	3.87	3.50	3.53	3.58	3.60	3.50
Cr_2O_3	0.24	0.17	0.17	0.11	0.14	0.18	0.18	0.14	0.15
Al_2O_3	18.49	18.76	18.98	18.76	19.20	18.97	18.82	18.94	19.04
FeO	20.54	20.59	20.39	20.55	20.55	20.48	20.31	21.06	20.26
MnO	0.06	0.07	0.11	0.10	0.10	0.08	0.05	0.12	0.10
NiO	0.07	0.03	0.04	0.04	0.03	0.00	0.02	0.07	0.06
MgO	7.39	7.16	7.76	7.40	7.41	7.38	7.25	7.43	7.39
CaO	0.00	0.00	0.01	0.00	0.00	0.00	0.00	0.00	0.00
Na_2O	0.14	0.17	0.20	0.14	0.18	0.25	0.14	0.16	0.15
K_2O	9.36	9.43	9.34	9.58	9.37	9.27	9.48	9.38	9.38
Total	94.64	94.56	95.14	95.50	95.20	94.84	94.40	95.18	95.08
Cations									
Si	2.76	2.74	2.75	2.76	2.75	2.75	2.76	2.72	2.78
Ti	0.22	0.23	0.20	0.23	0.21	0.21	0.22	0.22	0.21
Cr	0.02	0.01	0.01	0.01	0.01	0.01	0.01	0.01	0.01
Al	1.75	1.78	1.78	1.76	1.80	1.79	1.78	1.78	1.79
Fe^{2+}	1.38	1.38	1.35	1.37	1.37	1.37	1.36	1.40	1.35
Mn	0.00	0.00	0.01	0.01	0.01	0.01	0.00	0.01	0.01
Ni	0.00	0.00	0.00	0.00	0.00	0.00	0.00	0.00	0.00
Mg	0.88	0.86	0.92	0.88	0.88	0.88	0.87	0.88	0.88
Ca	0.00	0.00	0.00	0.00	0.00	0.00	0.00	0.00	0.00
Na	0.02	0.03	0.03	0.02	0.03	0.04	0.02	0.02	0.02
K	0.96	0.97	0.95	0.97	0.95	0.95	0.97	0.95	0.95
Total	8.00	8.00	8.00	8.00	8.00	8.00	8.00	8.00	8.00
Ratios and site activities									
xMg/(Fe^{2+})	0.39	0.38	0.40	0.39	0.39	0.39	0.39	0.39	0.39
xMg/(Fe^{tot})	0.39	0.38	0.40	0.39	0.39	0.39	0.39	0.39	0.39
Σcations	8.00	8.00	8.00	8.00	8.00	8.00	8.00	8.00	8.00
Charge Def.	–0.74	–0.73	–0.71	–0.75	–0.74	–0.74	–0.75	–0.68	–0.79
$xFe^{(tot)}$	0.61	0.62	0.60	0.61	0.61	0.61	0.61	0.61	0.61

M – mesosome, L – neosome

4.2.3. Toorongo contact hornfels (sample 201)

Described in section 4.1.

5. Approach and methodology

5.1. Pseudosection modelling

Pseudosection modelling and estimation of the P–T conditions of metamorphism of the Toorongo contact aureole hornfels were carried out using the computer program THERMOCALC 3.25 (Powell et al. 1998) and an internally consistent thermodynamic database (Powell and Holland 1993).

Pseudosections were constructed in the Mn–Na_2O–CaO–K_2O–FeO–MgO–Al_2O_3–SiO_2–H_2O–TiO_2–O + silicate melt (MnNCKFMASHTO) system and water was assumed to be in excess. The amount of water was taken as 5 vol. %, required to saturate the studied pelitic

assemblage at its solidus. Although melting processes in metapelites and metagreywackes can be modelled in the NCKFMASH system, the presence of Fe–Ti oxides and Ti-bearing biotite requires the use of the MnNCKFMASHTO system. The calculation involves the minerals quartz, sillimanite, orthopyroxene, ilmenite, K-feldspar, plagioclase, cordierite, garnet, biotite, magnetite and muscovite. The thermodynamic model and a–x model employed were those of Holland and Powell (1998 – cordierite), Holland and Powell (2003 – K-feldspar and plagioclase), Coggon and Holland (2002 – muscovite), White et al. (2007 – biotite), White et al. (2002 – magnetite, ilmenite). The garnet model used is a combination of the a–x models of White et al. (2001) and White et al. (2002).

The amount of free oxygen was taken as 0.05 vol. % in order to maintain Fe–Ti oxide stability over the entire P–T range. For the precise estimation of H_2O and O_2, T–X pseudosections are required.

Tab. 3 Selected mineral analyses of cordierite, muscovite and K-feldspar (wt. % and apfu)

	Crd-L	Crd-L	Ms-L	Ms-L	Kfs-M	Kfs-M	Kfs-M
No	27-r	28-c	51	41	16-r	17-c	18-c
SiO_2	47.91	47.24	43.65	45.50	64.394	63.941	64.482
TiO_2	0.00	0.01	0.02	0.03	0.000	0.028	0.009
Cr_2O_3	0.03	0.00	0.00	0.01	0.000	0.000	0.000
Al_2O_3	32.40	32.52	33.84	35.55	18.556	18.588	18.422
FeO	11.15	11.01	4.68	1.27	0.144	0.175	0.148
MnO	0.17	0.16	0.04	0.00	0.000	0.022	0.000
NiO	0.03	0.00	0.04	0.00	0.037	0.016	0.000
MgO	6.78	6.86	2.21	0.72	0.000	0.008	0.007
CaO	0.00	0.02	0.00	0.00	0.033	0.018	0.009
Na_2O	0.17	0.16	0.55	0.56	2.340	1.797	2.072
K_2O	0.00	0.00	8.96	10.53	13.227	14.129	13.701
Total	98.72	98.07	94.03	94.25	98.83	98.73	98.95
Cations (Fe^{2+}/Fe^{3+} charge balance)							
Si	4.97	4.93	2.96	3.06	2.98	2.97	2.99
Ti	0.00	0.00	0.00	0.00	0.00	0.00	0.00
Cr	0.00	0.00	0.00	0.00	0.00	0.00	0.00
Al	3.96	4.00	2.70	2.82	1.01	1.02	1.01
Fe^{3+}	0.13	0.18	0.23	0.03	0.01	0.01	0.01
Fe^{2+}	0.84	0.78	0.04	0.04	0.00	0.00	0.00
Mn	0.01	0.01	0.00	0.00	0.00	0.00	0.00
Ni	0.00	0.00	0.00	0.00	0.00	0.00	0.00
Mg	1.05	1.07	0.22	0.07	0.00	0.00	0.00
Ca	0.00	0.00	0.00	0.00	0.00	0.00	0.00
Na	0.03	0.03	0.07	0.07	0.21	0.16	0.19
K	0.00	0.00	0.77	0.90	0.78	0.84	0.81
Total	11.00	11.00	7.00	7.00	5.00	5.00	5.00
End members							
Anorthite					0.00	0.00	0.00
Albite					0.21	0.16	0.19
K-feldspar					0.79	0.84	0.81
Total end members					1.00	1.00	1.00
X(Fe/(Fe+Mg))	0.48	0.47	0.54	0.50			

M – mesosome, L – neosome; r – rim, c – core
Crd – cordierite, Ms – muscovite, Kfs – K-feldspar

5.2. Whole-rock geochemistry

The bulk-rock composition of the hornfels/migmatite (sample 201) for the pseudosection modelling was determined by XRF spectrometry at James Cook University, Townsville, and is presented in Tab. 4. Clean fresh fragments of samples were crushed in a bench jaw crusher and further pulverised in a tungsten mill. Approximately 2 grams (in duplicate) of each sample were ignited in a muffle furnace at 1000 °C for minimum of 4 hours to determine Loss on Ignition (LOI). One (1.0000 ± 0.0050) gram of ignited sample was mixed with eight (8.0000 ± 0.0050) grams of Norrish–Hutton flux and fused in a Pt crucible for 10 minutes at 1100 °C. This produces a homogeneous glass bead 40 mm in diameter. The specimens were analysed in a Bruker-AXS S4 Pioneer XRF spectrometer; data collected from various scan ranges were processed through Bruker-AXS Spectra-plus Software. The check standard run with these samples was AGV-2 (Silicates General).

5.3. Electron-probe microanalysis (EPMA)

The electron-microprobe analysis of selected minerals was carried out at the Microbeam Laboratory hosted by the University of the Melbourne using a Cameca SX 50 electron microprobe with four vertical wavelength-dispersive (WDS) spectrometers. Analysing crystals used were: for heavy elements (Fe, Cr, Mn) LiF (Lithium Fluoride) 100 crystal with d-spacing of 4.026 Å; for intermediate elements (Ti, Ca, K) PET (Polyethylene Terrephthalate) crystal with d-spacing of 8.75 Å and for light elements (Si, Mg, Al, Na, P) TAP (Thallium Acid Phthalate) crystal with d-spacing of 25.745 Å, all using K_α X-ray lines. Analyses were carried out using beam current of 35 nA, accelerating voltage of 15 kV, tilt angle and also the azimuth angle of 0. Counting time for all elements was 20 s on peak, 10 s on two backgrounds on either side of the peak position. Detec-

Tab. 4 Major-element compositions (wt. %) of hornfelses from the Toorongo contact aureole: 201 (related to whole rocks including mesosome and neosome) and 206 (for comparison)

Sample No	SiO_2	TiO_2	Al_2O_3	Fe_2O_3	MnO	MgO	CaO	Na_2O	K_2O	P_2O_5	LOI	Total	ASI	Σ oxides
201	64.2	0.8	17.73	5.97	0.06	2.50	0.48	1.00	5.27	0.14	1.60	99.72	2.2	98.12
206	83.1	0.4	7.65	2.39	0.04	1.05	0.31	0.81	1.53	0.09	1.86	99.30	2.2	97.44

All Fe is calculated as Fe_2O_3

tion level for all elements is better than 0.05 elemental weight percent (500 ppm).

The raw data were recalculated to mineral formulae using in-house EXCEL spreadsheets; the mineral formulae are based on 8 (feldspars), 11 (micas) and 18 (cordierite) oxygen atoms per formula unit (apfu). The Fe^{2+}/Fe^{3+} ratio was calculated using stoichiometric considerations.

Tab. 5 Measured values of Ti (ppm) as a function of spot size (μm) compared to the recommended value for standard AGV2

Sample	Spot size (μm)	Ti (ppm)
AGV2	30	7398
AGV2	55	8075
AGV2	80	7399
AGV2	110	7169
Recommended value		6300

5.4. TitaniQ

Cathodoluminescence images of quartz from the Tynong hybrid quartz diorite, Toorongo granodiorite and Toorongo contact aureole hornfels were obtained from carbon-coated polished sections at the CSIRO, Division of Minerals, Melbourne, Australia.

These rocks were studied for quantification of Ti in quartz by EPMA and LA ICP-MS. The CL system was attached to a JEOL JXA 8500F Hyper-probe. The CL system used is a spectral system by which full spectra at each pixel were collected without using any RGB filters, and the images were fitted to the peak of Ti^{4+}. Imaging was carried out at an accelerating voltage of 20 kV, and beam current of 40 nA and Ti contents were estimated at 20 kV, 150 nA, 10 μm spot, 80 seconds on peak. The outputs from two PE spectrometers were summed for the Ti measurements which gave a 3σ detection limit of ~15 ppm and precision of 10 %, which in temperature calculations is *c.* 50 °C using Huang and Audetat's (2012) calibration. Two TAP crystals were summed together to determine whether Al was associated with any of the peaks.

Titanium concentrations were determined via laser ablation ICP-MS on polished thick sections (~50–60 μm), using a New Wave UP 213 nm Nd:YAG laser ablation microprobe coupled with a Thermo Finnigan X series II, quadrupole ICP-MS at the School of Earth, Atmosphere and Environment, Monash University. Analyses were carried out in a helium atmosphere, employing a pulse rate of 5 Hz and beam energy of ~5 J/cm² at the sample. Laser spot size was ~30 μm. Background readings were collected for 30 s followed by 60 s ablation time. The raw LA ICP-MS data were reduced using the GLITTER 4.0 software package (Van Achterbergh et al. 2001) and quantitative results for Ti were obtained using the NIST 612 glass as an external standard. Silica concen-

Tab. 6 Summary of the P–T conditions estimated in this study

	Temperature, °C				Pressure, kbar
	Maximum	Minimum	Maximum	Minimum	
By pseudosection modelling, sample 201					
Entire possible ranges	750	650			1.0–4.3
x(Fe/(Fe + Mg)) of biotite	750	690			1.3–3.3
x(Fe/(Fe + Mg)) of cordierite	750	690			1.3–3.3
An content of plagioclase	710	660			2.5–4.4
By TitaniQ using $aTiO_2 = 0.5$	Huang and Audetat (2012)		Zhang et al. (2020)		
ocellar quartz in sample 802-1 using Ti analyzed by EPMA	900	630	830	550	2.5
ocellar quartz in sample 802-1 using Ti analyzed by LA ICP-MS	830	695	750	620	2.5
non-ocellar quartz in sample 802-1 using Ti analyzed by LA ICP-MS	860	780	790	700	2.5
quartz in sample 203 using Ti analyzed by LA ICP-MS	830	690	750	620	2.5
quartz in sample 201 using Ti analyzed by LA ICP-MS	790	610	710	535	2.5
By TitaniQ using $aTiO_2 = 0.8$	Huang and Audetat (2012)		Zhang et al. (2020)		
ocellar quartz in sample 802-1 using Ti analyzed by EPMA	830	585	775	510	2.5
ocellar quartz in sample 802-1 using Ti analyzed by LA ICP-MS	760	650	690	570	2.5
non-ocellar quartz in sample 802-1 using Ti analyzed by LA ICP-MS	790	650	720	570	2.5
quartz in sample 203 using Ti analyzed by LA ICP-MS	760	640	690	570	2.5
quartz in sample 201 using Ti analyzed by LA ICP-MS	730	570	750	500	2.5

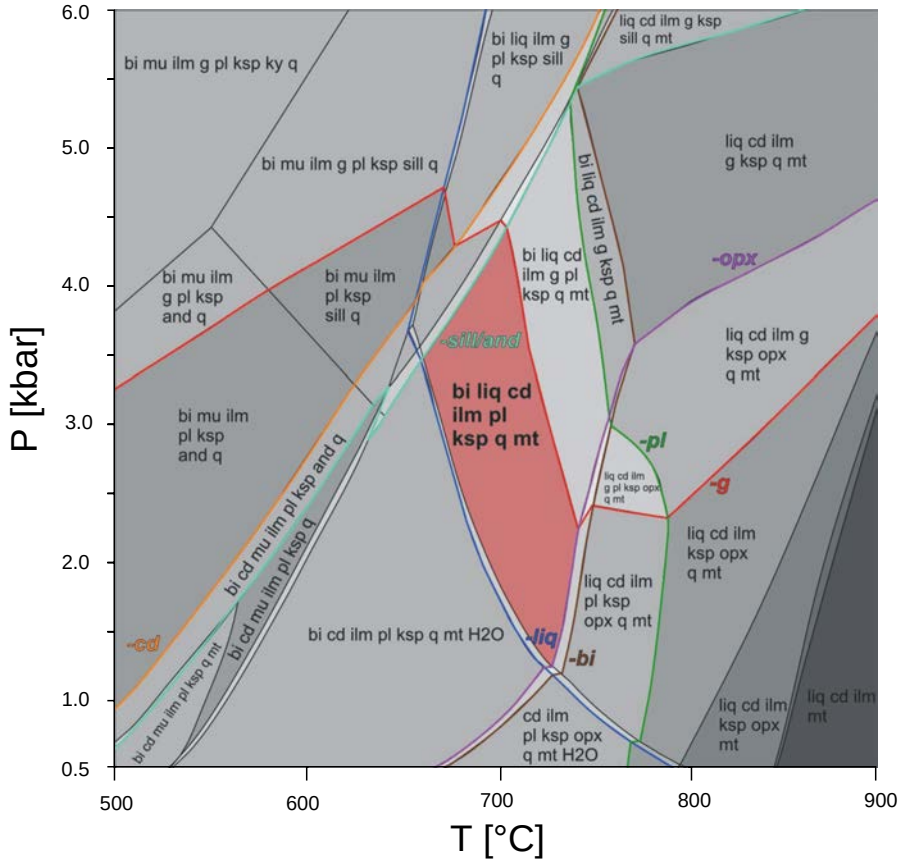

Fig. 5 P–T pseudosection of the hornfels sample 201. The red field represents that corresponding to the modal composition of the rock. The blue line marks the solidus.

trations obtained by electron microprobe were used for internal standardization. Based on comparison between our analyses and recommended values for standards, Ti concentrations were subsequently corrected for the difference between the measured and recommended values for the USGS glass standards BCR2 and AGV2 that were analysed throughout the analytical sessions and were used for quality control. The typical detection limit of the LA ICP-MS is 2–3 ppm, and precision is *c.* 10 %, which in temperature calculations corresponds to *c.* 40–50 °C using Huang and Audetat's (2012) calibration. The correction factor for sample 802-1 was −23 % and for samples 203 and 201 was −24 %. The magnitude of these corrections could theoretically introduce additional uncertainty of approximately 150 °C, when propagated. Table 5 shows measured Ti values on glass standard AGV2 for different spot sizes and the recommended Ti concentration of AGV2.

The activity of titanium is the most difficult parameter to establish (Campbell et al. 2009). An extensive search was made for the presence of rutile in our samples with no success. However, iron–titanium oxides (ilmenite and sphene) are present in the analysed samples. In the presence of such minerals, it is estimated that TiO_2 activities in silicic melts at typical magmatic temperatures are generally 0.5 or higher (Hayden and Watson 2007). Activity values lower than 0.5 are probably rare in most silicic magmas because of the presence of Ti-bearing minerals such as ilmenite and sphene (Watson et al. 2006). So the calculations were done using Huang and Audetat (2012) and Zhang et al. (2020) calibrations, taking the activities of titanium ($a\mathrm{TiO_2}$) of 0.5 and 0.8 as endmember cases. However, Ghiorso and Gualda (2013) reached the conclusion that $a\mathrm{TiO_2}$ varies with the liquid composition and temperature of the magma.

6. Results

Summary of results of the pressure and temperature estimated by various methods in this study is given in Tab. 6.

6.1. Pseudosection P–T modelling

The results of pseudosection modelling are given in Figs 5–8. Figure 5 shows that the stability field corresponding to the mineral assemblage of the hornfels 201 (i.e. biotite, cordierite, K-feldspar, plagioclase, magnetite, ilmenite, quartz and melt) is quadrivariant and covers possible pressures (P) between *c.* 1.0 and 4.3 kbar, and temperatures (T) between 650 and 750 ± 20 °C. Muscovite is stable mainly below the solidus and breaks down with the appearance of melt, but a narrow field of muscovite

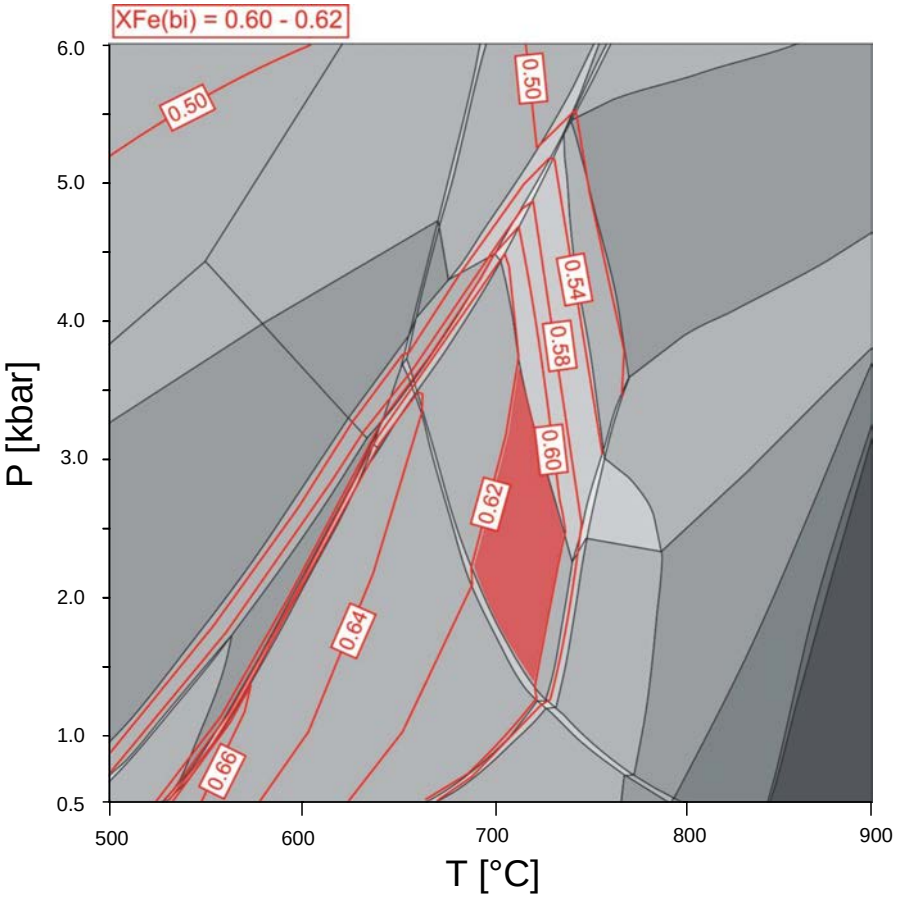

Fig. 6 P–T pseudosection as in Fig. 5 with x(Fe/(Fe + Mg)) isopleths for biotite. The red field marks a subsection of the larger field determined in Fig. 5, limited by the x(Fe) composition of biotite varying between 0.60 and 0.62 (see Tab. 2).

and liquid is present at >3.5 kbar. The presence of muscovite is interpreted to be the result of retrograde metamorphism, as it shows skeletal texture that is assumed to be formed at the expense of other minerals. The isopleths are temperature-dependent above the solidus. Increasing temperature above the solidus leads to the disappearance of biotite, followed by quartz, then plagioclase and finally K-feldspar. Most of the reactions are pressure-dependent but not strongly temperature-dependent. In order to further constrain the melting conditions of this sample, we calculated mineral composition isopleths for biotite, cordierite and plagioclase, as shown in Figs 6–8, and compared them to the compositions of these minerals in the rock listed in the Tabs 1–3.

The isopleths represent the Fe/(Fe + Mg) ratios of biotite (Fig. 6) and cordierite (Fig. 7), and the anorthite content of plagioclase (Fig. 8). Temperatures based on the x(Fe/(Fe + Mg)) of biotite (0.60–0.62) and cordierite (0.47–0.48) are similar to each other (690–750 °C), whereas those estimated from the anorthite content of plagioclase (Fig. 8) are lower (*c.* 660–710 °C), but the difference is not statistically significant. Pressure estimates are similar for biotite and cordierite (*c.* 1.3–3.6 kbar), whereas they are considerably higher for plagioclase (*c.* 2.5–4.4 kbar).

6.2. TitaniQ geothermometry

We combined CL images and the TitaniQ method to investigate the three samples described in section 4.2. Temperature estimates presented in Tab. 6 and in the text were calculated using expressions 3 and 4 above, with $a\mathrm{TiO_2}$ = 0.5 and 0.8 and a pressure of 2.5 kbar, the latter compatible with the pressure ranges obtained from pseudosection modelling.

6.2.1. Tynong hybrid diorite

Cathodoluminescence imaging of an ocellar quartz grain shows that it is patchily zoned (Fig. 9a) with the CL intensity decreasing from core to margin. Corresponding Ti contents analyzed first by EPMA ranged from 151 to 17 ppm (Electronic supplementary material, ESM 1a). The calculated core to margin temperature ranges indicated for this grain using expressions 3 and 4 are 900–630 and 830–550 °C ($a\mathrm{TiO_2}$ = 0.5) and 830–590 and 770–510 °C ($a\mathrm{TiO_2}$ = 0.8) (Fig. 9b). The same ocellar grain was analyzed using LA ICP-MS, with Ti contents varying from 94 to 33 ppm (ESM 1b) and corresponding temperature ranges of 830–700 and 750–620 °C ($a\mathrm{TiO_2}$ = 0.5) and 760–650 and 690–570 °C ($a\mathrm{TiO_2}$ = 0.8) (Fig.

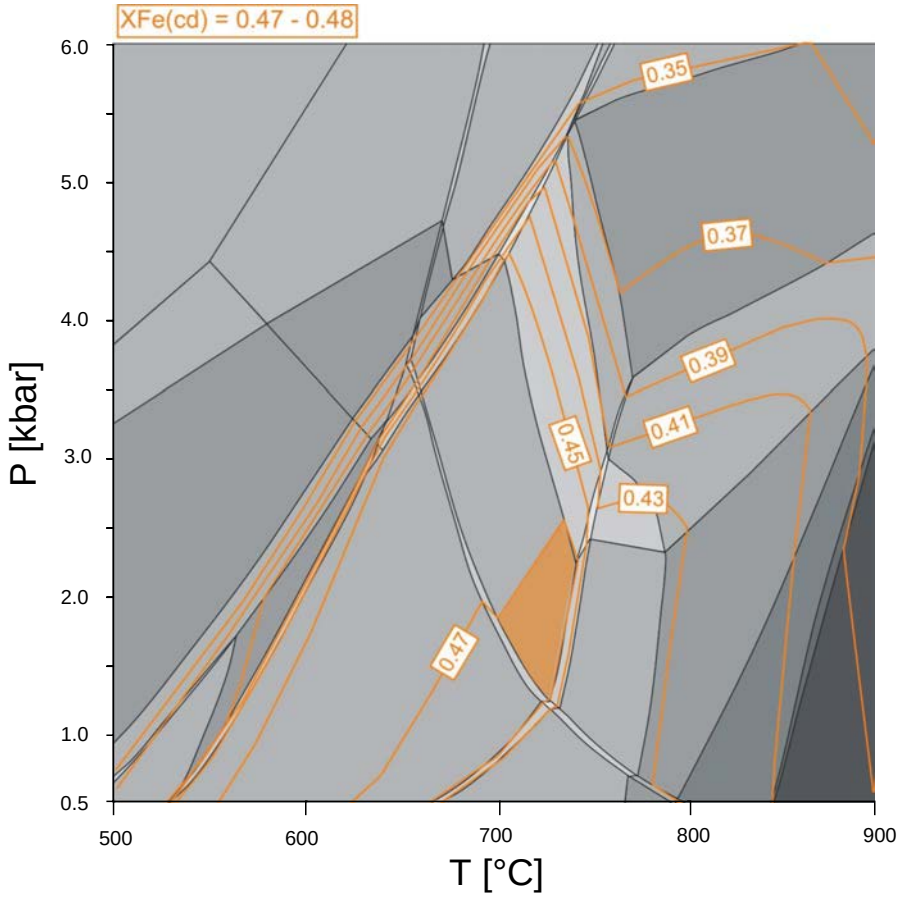

Fig. 7 P–T pseudosection as in Fig. 5 with x(Fe/(Fe + Mg)) isopleths for cordierite. The orange field marks a subsection of the larger field determined in Fig. 5, limited by the x(Fe) composition of cordierite varying between 0.47 and 0.48 (Tab. 3). Note that the field coincides closely with that for biotite shown in Fig. 6.

9c). Hence the overall extremes of indicated temperature for this grain are *c.* 900 and 510 °C (Tab. 6). A profile of ocellar quartz shows a systematic decrease of temperature from core to margin (Fig. 9d). The difference in Ti contents analysed by EPMA and LA ICP-MS may be due to the use of distinct analytical spots for the two methods.

Similarly, for quartz that is not ocellar, Ti concentration analysed by LA ICP-MS vary from 117 to 65 ppm, with a corresponding temperature ranges using expression 3 and expression 4 at Ti activity of 0.5 and 0.8 are 860–780 °C and 790–700 °C (0.5) (ESM 1b) and 790–650 °C and 720–570 °C (0.8). In contrast to an ocellar quartz, a non-ocellar quartz grain studied does not show margin ward decrease of Ti and calculated temperature (Fig. 9c–d).

6.2.2. Toorongo granodiorite

The CL image of quartz from the Toorongo granodiorite shows patchy zoning (Fig. 10a). There is nevertheless a high luminescence core showing higher Ti concentration. Contents of Ti analysed by LA ICP-MS vary from 94 to 29 ppm and the corresponding temperature ranges calculated using expressions 3 and 4 are 830–690 °C and 750–620 °C ($aTiO_2$ = 0.5) (Fig. 10b–c) (ESM 2) vs. 760–640 °C and 690–570 °C ($aTiO_2$ = 0.8) (Fig. 10b–c). Analyses located near biotite show low Ti, indicating that co-precipitation of biotite may have affected the Ti content of quartz (ESM 2).

6.2.3. Hornfels from the Toorongo contact aureole

Cathodoluminescence examination of the neosome of the hornfels shows that quartz is weakly zoned, again with higher temperature cores and lower temperature rims (Fig. 11a). Some grains have lower temperature cores associated with inclusions of opaque minerals (Fig. 11a). Titanium concentrations analysed by LA ICP-MS vary from 70 to 11 ppm that, using expressions 3 and 4, yield temperature ranges of 790–610 °C and 710–635 °C ($aTiO_2$ = 0.5; ESM 3) (Fig. 11b–c). The temperatures decrease towards the margin and in the vicinity of opaque inclusions (Fig. 11a, c). The temperatures range calculated for Ti activity of 0.8 are 730–570 °C and 750–490 °C (Fig. 11b–c).

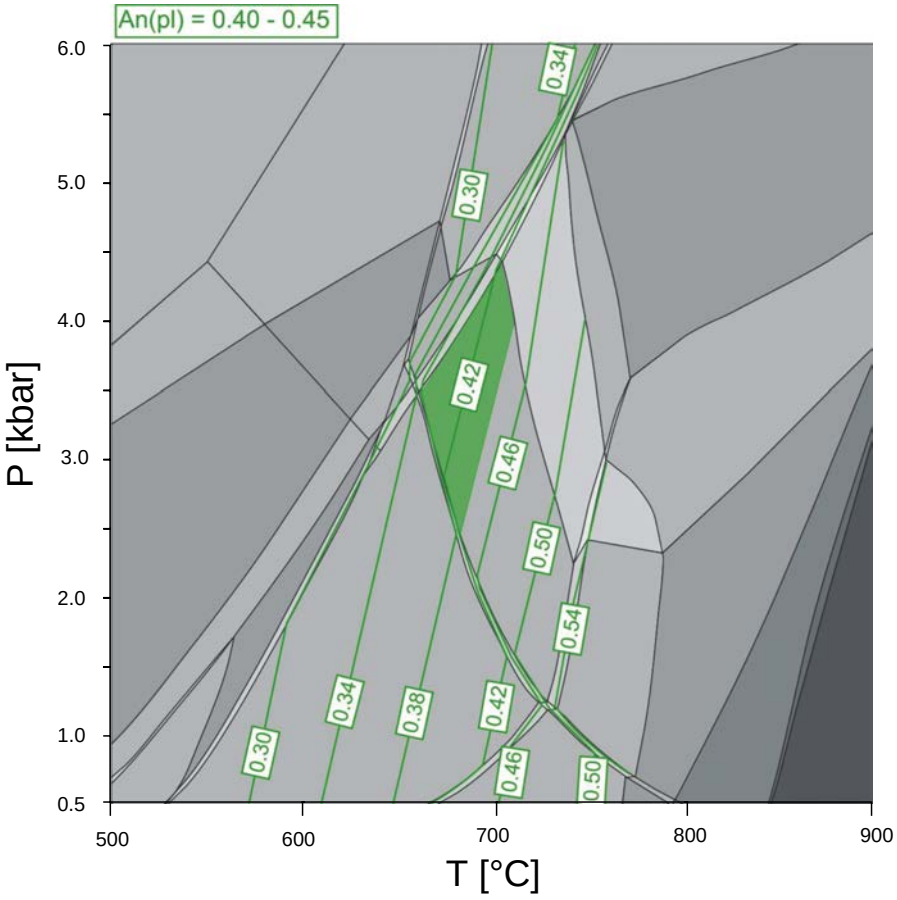

Fig. 8 P–T pseudosection as in Fig. 5 with anorthite isopleths for plagioclase. The green field marks a subsection of the larger field determined in Fig. 5, limited by the An content of plagioclase (0.40–0.45, Tab. 1). Note that unlike Figs 6 and 7, in this case the smaller field lies in the higher pressure and lower temperature section of the larger field of Fig. 5.

7. Discussion

7.1. Pseudosection modelling

Using the fields indicated by the composition of the biotite and cordierite, we are able to narrow the estimated temperature and pressure of melting of the Toorongo contact aureole hornfels to 690–750 °C and 1–3 kbar, respectively. From this we conclude that the Toorongo Pluton was emplaced at shallow depths of approximately 4–10 km. However, there are several uncertainties that complicate the P–T estimates. In particular, as previously noted, the XRF analysis does not take into account melt extracted from the hornfels that may have changed the original bulk composition of the rock. The SiO_2 content and alkalis of the residues will have been lowered but alumina will have increased because feldspars produced by melting are sodium-rich and have relatively low alumina. If melt was removed from the protoliths, peritectic minerals will have gone into the melt.

The pressure–temperature conditions estimated from the anorthite content of plagioclase (Fig. 8) are not consistent with those obtained using biotite (Fig. 6) and cordierite (Fig. 7). This may be due to: a) changing rock chemistry due to melt loss impacting on the fields in the pseudosection and the position of the isopleths, and/or b) re-equilibration of plagioclase during change in bulk-rock and melt chemistry. The range of anorthite contents in plagioclase of the sample 201 is 0.28 to 0.45 (Tab. 1). However, in Fig. 8 only the higher anorthite values (0.40 to 0.45) plot within the field in which melting occurs. Combined with significant normal zonation in plagioclase this is taken to indicate that the chemistry of the system was evolving. Zonation toward low An contents implies that the system may have been cooling and decompressing towards melt-out conditions during uplift. Similar zonation is not seen in either cordierite or biotite. These minerals may have re-equilibrated more rapidly during decompression.

Another source of uncertainty in the pseudosection treatment relates to the regions below the solidus. These may be inaccurate because the amount of water in the calculations was kept fixed. The amount of water and oxygen ideally must be estimated from T–X pseudosections.

7.2. TitaniQ geothermometry

Results for the three studied samples cover approximately the same temperature range, from ~900 °C in cores of quartz crystals to ~610 °C ($a\mathrm{TiO_2}$ = 0.5) at their margins and

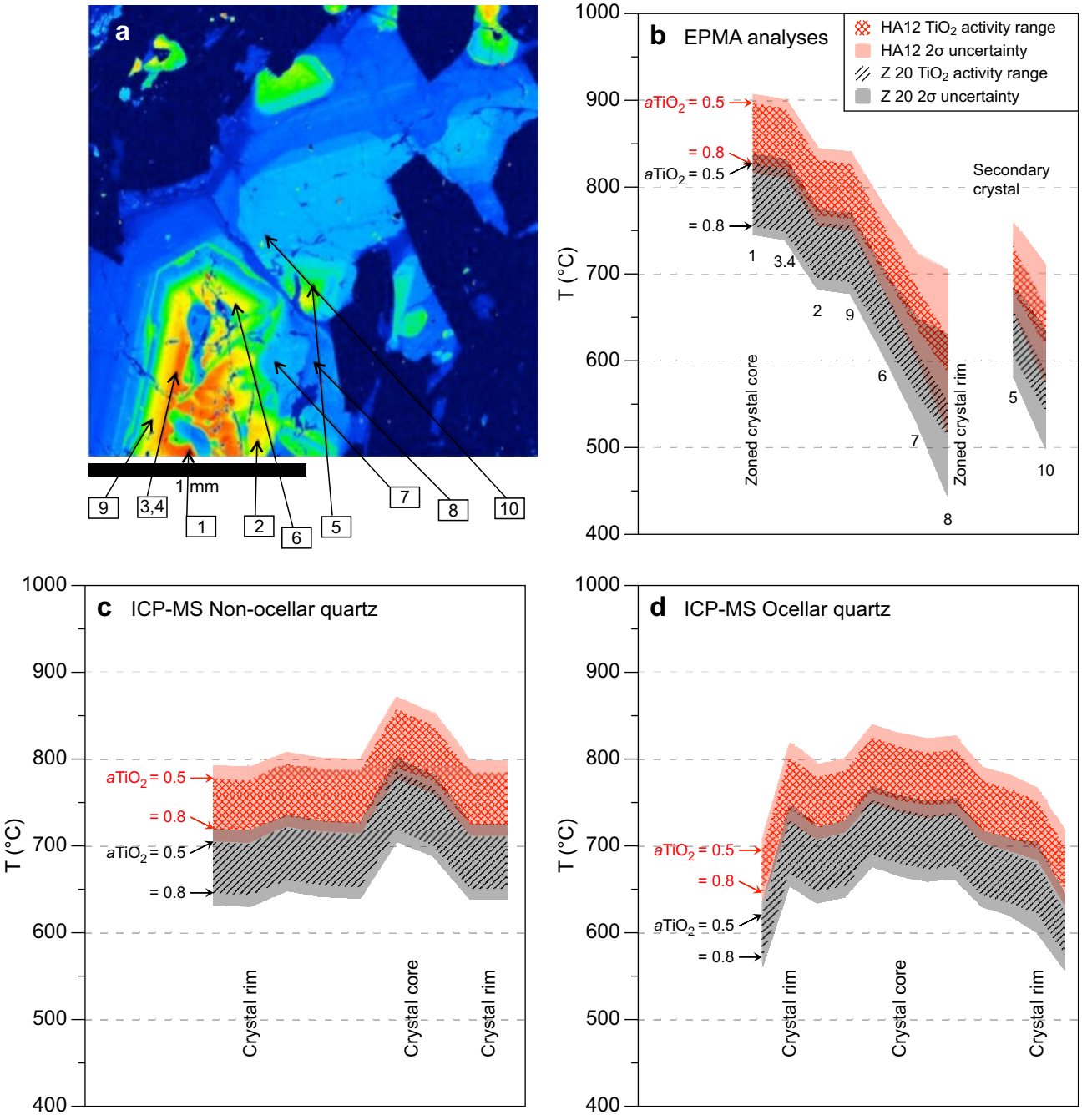

Fig. 9 Crystallization temperatures of quartz grains from sample 802-1 (Tynong hybrid quartz diorite) estimated by TitaniQ thermometry using calibrations of Huang and Audetat (2012) and Zhang et al. (2020) at Ti activities of 0.5 and 0.8. **a** – Cathodoluminescence image of quartz (numbers indicate the analysis points for which data are given in ESM 1a). Color gradient depicts detected CL intensity, with red corresponding to highest Ti contents; **b** – Temperature profiles of quartz from quartz ocelli based on Ti concentrations analysed by EPMA, where point labels correspond to analytical positions in ESM 1a, and are arranged in stratigraphic order from core to rim. **c–d** – Temperature profiles of quartz without ocellar jackets (**c**) and from a quartz ocellus (**d**) based on Ti concentrations analysed by LA ICP-MS. The tracks (not shown in (**a**)) were more or less straight lines from margin to core to margin. Abscissa represents analysis order along the traverse, but distance is not to scale. Abbreviations used here and in subsequent figures: HA12: Huang and Audetat (2012) and Z20: Zhang et al. (2020).

from 830 to 570 °C ($a\mathrm{TiO_2}$ = 0.8) using expression (3). The results of the temperature estimation using expression (4) yield values from 830 to 540 °C ($a\mathrm{TiO_2}$ = 0.5), while they range from 775 to 500 °C ($a\mathrm{TiO_2}$ = 0.8). As a comparative example, Kairi et al. (2012) have compiled crystallization temperatures for rapakivi granites of the Fennoscandian Peninsula, determined by a variety of methods, ranging from 670 to 800 °C. Given the probable uncertainties of 20–50 °C associated with the methods used in calculated temperatures using the expression calibrated by Huang and

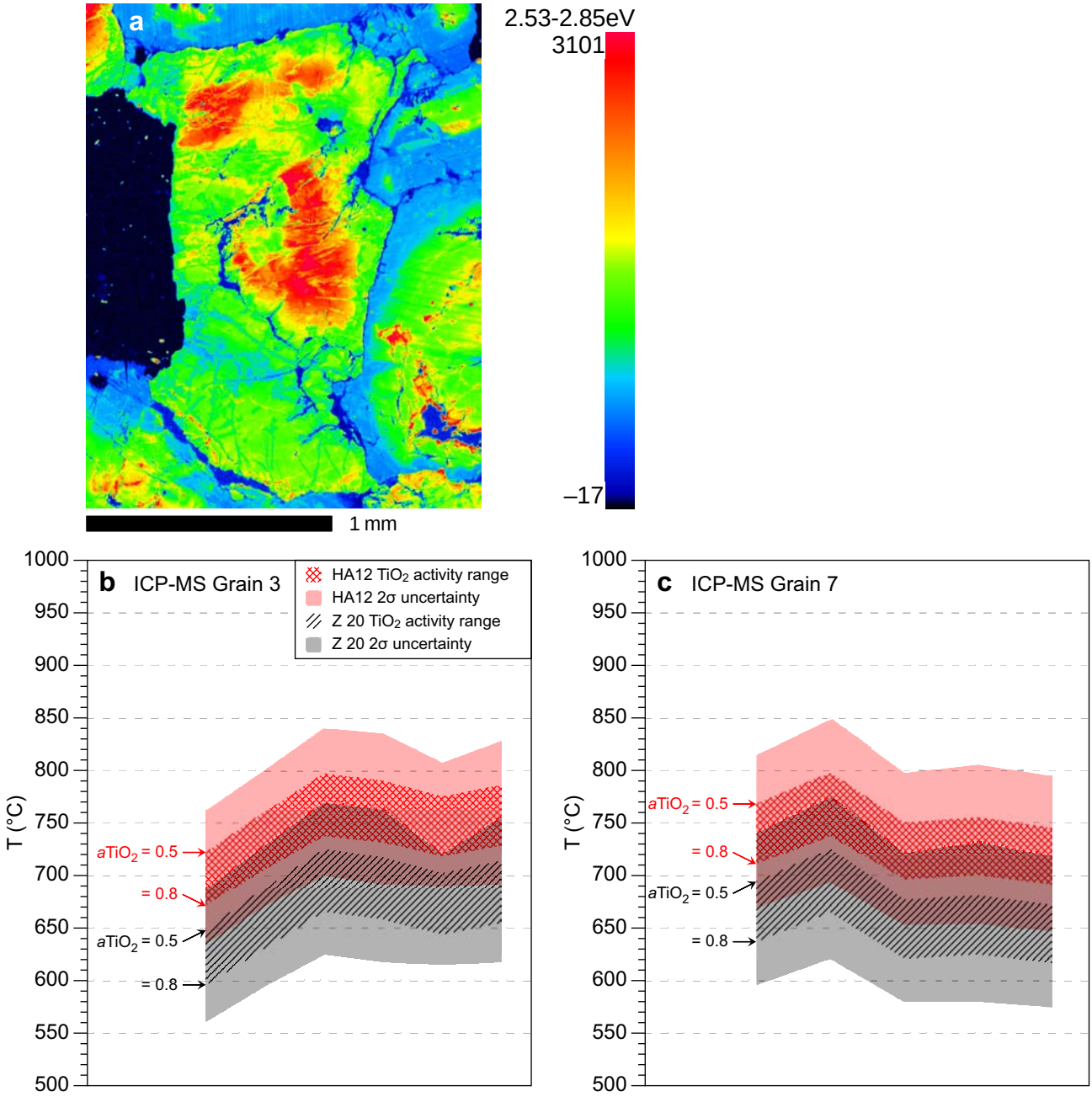

Fig. 10 Calculated temperatures of quartz from sample 203 (Toorongo granodiorite) using calibration of Huang and Audetat (2012) and Zhang et al. (2020) at Ti activity of 0.5 and 0.8. **a –** Representative CL image of quartz from sample 203; **b–c –** Temperature profiles of two quartz grains from sample 203 (grain 3, grain 7, ESM 2, not shown in **a**); where tracks were more or less straight lines from margin to core to margin. The abscissa is not to scale; 30 μm spot size.

Audetat (2012), the results obtained do not confirm unusually high temperatures for the Tynong plutons.

An unexpected outcome of these temperature estimations is that those from the Zhang et al. (2020) calibration are consistently 60–70 °C lower than those from the Huang and Audetat calibration. In addition, temperatures for $a\mathrm{TiO_2}$ = 0.8 are consistently about 50 °C lower than for 0.5 for both calibrations. When these systematic differences are combined with analytical uncertainty for individual data (2 or 3σ for LA ICP-MS and EPMA, respectively) an overall uncertainty of the order of 150 °C is indicated.

The unexpectedly low temperatures derived from the Zhang et al. (2020) calibration, especially at $a\mathrm{TiO_2}$ of 0.8, lead to a high proportion of results close to or below the granite water-saturated solidus. Relatively few are >750 °C and many are close to 500 °C.

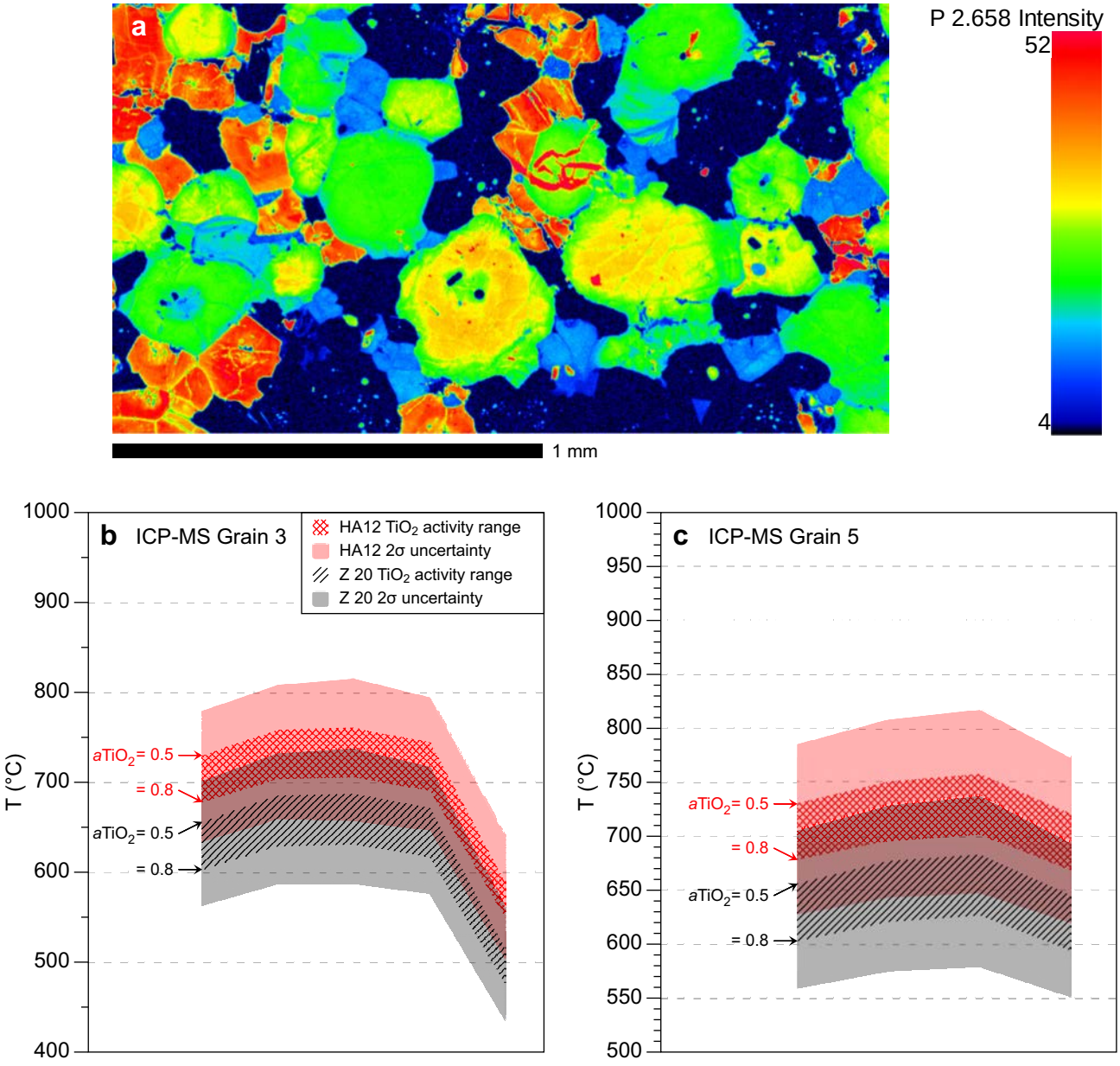

Fig. 11 Calculated temperatures of quartz from sample 201 (Toorongo hornfels) using calibration of Huang and Audetat (2012) and Zhang et al. (2020) at Ti activities of 0.5 and 0.8. **a –** Representative CL image of neosome showing CL intensity decreasing outwards within quartz crystals. Some grains have a central CL low, defining a doughnut shape; **b–c** Temperature profiles of quartz (grain 3 and grain 5, ESM 3, not shown in **a**); where tracks were more or less straight lines from margin to core to margin. The abscissa is not to scale.

7.3. Possibility of temperatures falling below the granite water-saturated solidus

Most of the analysed spots and calculated T using both Huang and Audetat (2012) and Zhang et al. (2020) approaches at $aTiO_2$ of 0.5 and 0.8 indicate temperatures below the granite water-saturated solidus. Even if a magma started out hot, quartz would be one of the last phases to crystallize, and the bulk of its crystallization would likely occur at the eutectic. Diffusion of Ti is relatively quick in Qtz, and therefore the potential for Ti incorporated at high T to leak out of quartz prior to closure with respect to diffusion is quite high. Cathodoluminescence reveals magmatic zoning (Fig. 9) in some quartz crystals and a smeared-out zonation that could be a result of diffusion in others (Fig. 10), meaning that at least the grains that have well-defined magmatic zoning likely record crystallization conditions. Therefore, in the absence of thermobarometry for early-crystallizing minerals the possibility cannot be excluded that the high-temperature part of the magma's history took place prior to the onset of quartz crystallization.

7.4. The sizes of plutons and the width of their contact aureoles

Even though the Toorongo Pluton as exposed is smaller than other plutons of the Tynong Province, apart from the Tanjil Bren Pluton, it has produced the widest contact aureole. Recently, modelling by Annen (2017) has confirmed that although the width of a contact aureole is primarily dependent upon the thickness of the intrusion which produced it, especially for sheet-like intrusions, other factors may play a prominent role. These include the relative rates of heat transfer within the intrusion and the country rocks and whether the country rocks contain significant water. Convective heat transport could in turn play a significant role in controlling the heat transfer rate within the intrusion.

If heat transfer is faster within the intrusion than in the country rocks, build-up of heat within the aureole may increase its width and lead to melting. This situation may have been the case for the Toorongo aureole. The Toorongo granodiorite is the most mafic of the Tynong plutons, and was therefore probably the hottest, making melting temperatures within the aureole relatively easier to reach.

Another potential factor noted by Annen (2017) is the maintenance of high temperatures within a pluton and its aureole due to the repeated injection of magma close to the contact. We have no direct evidence that this was the case for the Toorongo Pluton.

On the other hand, hydrothermal convection within water-bearing country rocks may lead to absorption of latent heat, inhibiting heat build-up and increase in temperature and hence limiting the thickness of the aureole. Annen (2017), however, considered this factor to be only of secondary importance.

Miller et al. (2003) calculated zircon saturation temperatures for granitoids and concluded that the typical range is 730–780 °C (an average of 766 ± 24 °C), with 800 °C rarely being exceeded. Our maximum temperature estimates for the Toorongo Pluton and its aureole by pseudosection modelling and TitaniQ geothermometry clearly fall into this range. On this basis we must conclude that the plutons of the Tynong Batholith were probably emplaced at temperatures within the upper part of the typical temperature range for granitoids and that melting of the Toorongo aureole may have been influenced by the thermal diffusivity of the country-rock greywackes being lower than that of the intrusion.

8. Conclusions

The results of THERMOCALC pseudosection modelling of tonalites–granites of the Tynong Batholith, Lachlan Orogen, southeastern Australia indicate that the pressure and temperature of metamorphism of the hornfels was approximately 1 to 3 kbar and 690 ºC to 750 ºC, respectively. This suggests that the Toorongo Pluton was emplaced at shallow depth. The temperature estimated by the THERMOCALC modelling at 1–3 kbar is similar to the average temperature estimated by TitaniQ geothermometry at 2.5 kbar and Ti activities ($a\mathrm{TiO_2}$) of 0.5 and 0.8. The pseudosection modelling and temperature estimation by using x(Fe) of cordierite and biotite yielded more realistic ranges and are comparable with temperature estimations made for biotite dehydration melting. The unrealistic temperature and pressure estimates indicated by the anorthite contents of plagioclase are possibly due to re-equilibration of plagioclase during melt loss.

Temperatures calculated using TitaniQ based on Ti concentration in quartz for magmatic rocks and a contact aureole hornfels for the Tynong Province are ~900–570 °C at $a\mathrm{TiO_2}$ of 0.5 and ~830–500 °C at $a\mathrm{TiO_2}$ of 0.8. We have shown that titanium concentrations are lowered in the vicinity of sulphides and oxides, as well as in later healed cracks within quartz grains. It can be concluded that the Tynong Batholith granitoids were not emplaced at temperatures as high as has been inferred from their mineral compositions and the melted contact aureole they have produced. Also, we conclude that the expression by Huang and Audetat (2012) yields more realistic temperature ranges for emplacement of these granitoids, while values obtained by pseudosection modelling provide just minimum estimates. It is worth mentioning that the calibration of Zhang et al. (2020) gives much lower temperature values than that of Huang and Audetat (2012).

Acknowledgments KRR is grateful to Monash University for a Monash Graduate Scholarship. An early version of the manuscript was greatly improved by comments from Professor Roberto Weinberg of Monash University. Constructive reviews by Andreas Audétat and Václav Špillar are highly acknowledged. John Hora and Vojtěch Janoušek are greatly acknowledged for their input in the early version of manuscript and editorial handling.

Electronic supplementary material. Supplementary tables of titanium concentrations (ppm) analysed by EPMA and LA ICP-MS as well as estimated temperatures are available online at the Journal web site (*http://dx.doi.org/10.3190/jgeosci.305*).

References

Annen C (2017) Factors affecting the thickness of thermal aureoles. Front Earth Sci 5: 82, doi 10.3389/feart.2017.00082

Bowen KG (1975) Potassium–argon dates – determinations carried out by Geological Survey of Victoria. Geological Survey of Victoria Reports 1975/3: Department of Mines, Victoria, pp 1–34

Campbell ME, Hanson JB, Minarik WG, Stix J (2009) Thermal history of the Bandelier Magmatic System: evidence for magmatic injection and recharge at 1.61 Ma as revealed by cathodoluminescence and titanium geothermometry. J Geol 117: 469-485

Cherniak DJ, Watson EB, Wark DA (2007) Ti diffusion in quartz. Chem Geol 236: 65–74

Clemens JD, Bezuidenhout A (2014) Origins of coexisting diverse magmas in a felsic pluton: the Lysterfield granodiorite, Australia. Contrib Mineral Petrol 167: 991, doi: 10.1007/s00410-014-0991-9

Clemens JD, Regmi K, Nicholls IA, Weinberg R, Maas R (2016) The Tynong Pluton, its mafic synplutonic sheets and igneous microgranular enclaves: the nature of the mantle connexion in I-type granitic magmas. Contrib Mineral Petrol 171: 35, doi: 10.1007/s00410-016-1251-y

Coggon R, Holland TJB (2002) Mixing properties of phengitic micas and revised garnet–phengite thermobarometers. J Metamorph Geol 20: 683–696

Connolly JAD, Petrini K (2002) An automated strategy for calculation of phase diagram sections and retrieval of rock properties as a function of physical conditions. J Metamorph Geol 20: 697–708

Ghiorso MS, Gualda GAR (2013) A method of estimating the activity of titania in magmatic liquids from the compositions of coexisting rhombohedral and cubic iron–titanium oxides. Contrib Mineral Petrol 165: 73–81

Gray C M, Kemp AIS (2009) The two-component model for the genesis of granitic rocks in southeastern Australia – nature of the metasedimentary-derived and basaltic end members. Lithos 111: 113–124

Hayden A, Watson EB (2007) Rutile saturation in hydrous siliceous melt and its bearing in Ti-thermometry of quartz and zircon. Earth Planet Sci Lett 258: 561–568

Holland TJB, Powell R (1998) An internally consistent thermodynamic dataset for phases of petrological interest. J Metamorph Geol 16: 309–343

Holland TJB, Powell R (2003) Activity–composition relations for phases in petrological calculations: an asymmetric multicomponent formulation. Contrib Mineral Petrol 145: 492–501

HOLNESS MB, WATT GR (2001) Quartz crystallization and fluid flow during contact metamorphism: a cathodoluminescence study. Geofluids 1: 215–228

Huang R, Audetat A (2012) The titanium-in-quartz (TitaniQ) thermobarometer: a critical examination and recalibration. Geochim Cosmochim Acta 84: 75–89

Kairi E, Evelin V, Juho K, Soesoo A (2012) Using a titanium-in-quartz geothermometer for crystallization temperature estimation of the Palaeoproterozoic Suursaari quartz porphyry. Est J Earth Sci 61: 195–204

Marmo BA, Clarke GL, Powell R (2002) Fractionation of bulk rock composition due to porphyroblast growth: effects on eclogite facies mineral equilibria, Pam Peninsula, New Caledonia. J Metamorph Geol 20: 151–165

McKenzie DA, Nott RJ, Bolger PR (1984) Radiometric age determination. Geological Survey of Victoria Reports 74: pp 1–63

Miller CF, McDowell SM, Mapes RW (2003) Hot and cold granites? Implications of zircon saturation temperatures and preservation of inheritance. Geology 31: 529–532

Müller A, Lennox P, Trzebski R (2002) Cathodoluminescence and micro-structural evidence for crystallisation and deformation processes of granites in the Eastern Lachlan Fold Belt (SE Australia). Contrib Mineral Petrol 143: 510–524

Otamendi JE, Patiño Douce AE (2001) Partial melting of aluminous metagreywackes in the Northern Sierra de Comechingones, central Argentina. J Petrol 42: 1751–1772

Powell R, Holland TJB (1993) On the formulation of simple mixing models for complex phases. Amer Miner 84: 1–14

Powell R, Holland TJB, Worley B (1998) Calculating phase diagrams involving solid solutions via non-linear equations, with examples using Thermocalc. J Metamorph Geol 16: 577–588

Regmi KR (2012) Petrology and Geochemistry of the Tynong Province Granitoids, Lachlan Orogen, Victoria, Australia. Unpublished PhD thesis, Monash University, Melbourne, pp 1–184

Regmi KR, Weinberg RF, Nicholls IA, Maas R, Raveggi M (2016) Evidence of hybridisation in the Tynong Province granitoids, Lachlan Fold Belt, eastern Australia. Aust J Earth Sci 63: 235–255

Rossiter AG (2003) Granitic rocks of the Lachlan Fold Belt in Victoria. In: Birch WD (ed) Geology of Victoria. Geological Society of Australia Special Publications 23: 217–237

Thomas JB, Watson EB, Spear FS, Shemella PT, Nayak, SK, Lanzirotti A (2010) TitaniQ under pressure: the effect of pressure and temperature on the solubility of Ti in quartz. Contrib Mineral Petrol 160: 743–759

Van Achterbergh E, Ryan CG, Jackson SE, Griffin WL (2001) Data reduction software for LA ICP-MS: Appendix. In: Sylvester PJ (ed) Laser Ablation-ICPMS in the Earth Sciences: Principles and Applications. Mineralogical Association of Canada (MAC) Short Course Series 29: 239–243

Vance D, Holland T (1993) A detailed isotopic and petrological study of a single garnet from the Gassetts schist, Vermont. Contrib Mineral Petrol 114: 101–118

Vandenberg AHM, Willman CE, Maher S, Simsons BA, Cayley RA, Taylor DH, Morand VJ, Moore DH, Radojkovic A (2000) The Tasman Fold Belt System in Victoria. Geological Survey of Victoria, Special Publications, Melbourne, pp 1–462

Wark DA, Watson EB (2006) TitaniQ: a titanium-in-quartz geothermometer. Contrib Mineral Petrol 152: 743–754

Watson EB, Wark DA, Thomas JB (2006) Crystallization thermometers for zircon and rutile. Contrib Mineral Petrol 151: 413–433

White RW, Powell R, Holland TJB (2001) Calculation of partial melting equilibria in the system Na_2O–CaO–K_2O–FeO–MgO–Al_2O_3–SiO_2–H_2O (NCKFMASH). J Metamorph Geol 19: 139–153

White RW, Powell R, Clarke GL (2002) The interpretation of reaction textures in Fe-rich metapelitic granulites of the Musgrave Block, central Australia: constraints from mineral equilibria calculations in the system K_2O–FeO–MgO–Al_2O_3–SiO_2–H_2O–TiO_2–Fe_2O_3. J Metamorph Geol 20: 41–55

White RW, Powell R, Holland TJB (2007) Progress relating to calculation of partial melting equilibria for metapelites. J Metamorph Geol 25: 511–527

Wiebe RA, Wark DA, Hawkins DP (2007) Insights from quartz cathodoluminescence zoning into crystallization of the Vinalhaven granite, coastal Maine. Contrib Mineral Petrol 154: 439–453

Wilson CJN, Seward TM, Allan ASR, Charlier LA, Bello L (2012) A comment on: 'TitaniQ under pressure: the effect of pressure and temperature on the solubility of Ti in quartz' by Thomas JB, Watson EB, Spear FS, Shemella PT, Nayak SK, Lanzirotti A. Contrib Mineral Petrol 164: 359–368

Zhang C, Li X, Almeev RR, Horn I, Behrens H, Holtz F (2020) Ti-in-quartz thermobarometry and TiO_2 solubility in rhyolitic melts: new experiments and parametrization. Earth Planet Sci Lett 538: 116213, doi: 10.1016/j.epsl.2020.116213